28th AIAA/CEAS Aeroacoustics 2022 Conference, June 14-17, 2022, Southampton, UK
DOI:10.2514/6.2022-3008

Exploring Angle of Attack Effects on the Aero-Acoustic Response of a Weapons Bay at Transonic and Supersonic Mach Number

David Bacci[1]
Oxford Thermofluids Institute, University of Oxford, Oxford, United Kingdom, OX2 0ES

Alistair J. Saddington[2]
Aeromechanical Systems Group, Cranfield University, Defence Academy of the UK, United Kingdom SN6 8LA

Numerical aero-acoustic analysis was conducted on a weapon bay model with doors, incorporating radar cross section reduction features. The effect of angle of attack on the aero-acoustic response of the cavity was analysed at a transonic Mach number of 0.85, and at a supersonic Mach number of 1.20. It was found that incidence had influence on both mean-flow features and acoustic response. Further, linear and angular accelerations induced by the flow on doors revealed potential adverse fluid-structure coupling when results were compared with modal analysis. Again, angle of attack did influence the aeroacoustic effects on the cavity door structure.

Nomenclature

f	=	frequency [Hz]
f_s	=	sampling frequency [Hz]
f_r	=	frequency resolution [Hz]
γ	=	ratio of specific heats for air
ω	=	angular velocity [rad/s]
$\dot{\omega}$	=	angular acceleration [rad/s^2]
M	=	Mach number
M_n	=	n_{th} structural mode
R_n	=	n_{th} acoustic resonant mode

[1]Research Fellow. Oxford Thermofluids Institute, Department of Engineering Science, University of Oxford.
[2] Reader. Aeromechanical Systems Group, Centre for Defence Engineering, Cranfield University.

RH_n = n_{th} Rossiter-Heller theory predicted mode

St = Strouhal number ($= f \cdot D/U$)

U = air speed

t_c = convective time ($= L/U_\infty$)

$\bar{x}$ = time averaged value of the discrete time series x_n ($\sum_{j=1}^{N} x_j/N$)

$\hat{X}$ = discrete Fourier transform of the variable x

X^* = complex conjugate of the variable X

μ_x = mean of variable x

σ_x = root mean square of variable x

p = air pressure

q = dynamic pressure

δ_0 = boundary layer thickness at cavity leading edge

ρ = air density

L = cavity length

W = cavity width

D = cavity dept

$\vec{u}$ = displacement vector of structure [m]

$\vec{\theta}$ = rotation vector of structure [rad]

m = mass [kg]

$\vec{I}$ = inertial tensor [kgm^2]

a = acceleration [m/s^2]

α = angle of attack [deg]

β = angle of sideslip [deg]

Subscripts

∞ = free-stream conditions

I. Introduction

DESIGN requirements for modern combat aircraft are strongly influenced by the reduction of radar signature. This implies that weapons must be carried inside the airframe, instead as suspended on the wing and fuselage. Whilst this solution offers advantages in terms of aerodynamic drag reduction (especially at transonic and supersonic speeds), other issues are generated because, during the weapon release procedure when the bay's doors are opened and the cavity is exposed to high speed flow, an intense acoustic field is developed capable of damaging the airframe and the payload. Additionally, the intrinsic unsteadiness of the local flow poses a hazard for the release of the weapon. The aeroacoustic response is directly related to cavity geometry and freestream conditions [1] and, in determined conditions, resonant modes are developed further aggravating the noise produced. The frequencies at which resonance occurs are called Rossiter modes, following early work on cavity flows [2]. The resonating frequencies are more generally predicted using the Rossiter-Heller equation [3], which accounts for Mach number effects,

$$f_n = \frac{U_\infty}{L} \cdot \frac{n - \xi}{M_\infty \left[1 + \frac{(\gamma - 1)}{2} M_\infty^2\right]^{-1/2} + \frac{1}{K}} \tag{1}$$

Here K is the ratio of disturbance velocity in the shear layer to the freestream velocity (generally taken as 0.57), and ξ is an empirical constant employed to account for the phase lag between the passage of an eddy past the cavity trailing edge and the formation of an upstream travelling disturbance. The value of ξ depends on the length-to-depth ratio (L/D) of the cavity and is evaluated as $\xi = 0.062(L/D)$ [2]. The ratio of specific heats, γ, is assumed to be equal to 1.4 for air.

As shown by Delprat [4], it is possible to express the resonating frequencies as the result of an amplitude modulation of a fundamental acoustic with relative harmonics:

$$f_n = (n - \xi) \cdot [f_a \pm k\Delta f] \tag{2}$$

Here, f_a is the fundamental frequency loop of the cavity (also called the "*carrier frequency*"), ξ is the amplitude modulation parameter, or the ratio of the amplitude modulation frequency f_b to f_a, Δf is a modulating frequency (which usually coincides with the low-frequency peaks in the spectrum), and k is an integer.

Knowing that the Rossiter-Heller equation formulation does not consider the modulating frequency Δf, it is possible to extract from the combination of Eq. (1) and (2) the direct dependence of f_a and f_b from cavity geometry and freestream conditions:

$$f_a = \frac{U_\infty}{L} \cdot \frac{1}{M_\infty \left[1 + \frac{(\gamma - 1)}{2} M_\infty^2\right]^{-1/2} + \frac{1}{K}} \tag{3}$$

$$f_b = \frac{U_\infty}{D} \cdot \frac{0.062}{M_\infty \left[1 + \frac{(\gamma - 1)}{2} M_\infty^2\right]^{-1/2} + \frac{1}{K}} \tag{4}$$

$$\xi = \frac{f_b}{f_a} = 0.062 \left(\frac{L}{D}\right) \tag{5}$$

Subsequent studies ([5],[6],[7]) allowed this set of frequencies to be associated with fluid structures inside the cavity. A typical open-type cavity, in which acoustic resonant frequencies are expected to appear, is characterised by a detached shear layer (located at the bay boundary with the external flow) forming at the leading edge and impinging at the trailing edge. Inside the cavity a recirculation area, typically defined by one or more eddies, is present. The well-known resonance phenomenon, involving the aero-acoustic loop, is usually associated with the cavity fundamental frequency f_a, and is strongly dependant on the cavity longitudinal dimension.

Re-arranging Eq.(3) in terms of St_D (i.e. Strouhal number based on cavity depth[3]) the following expression is obtained:

$$St_{D_a} = \frac{1}{\left(M_\infty \left[1 + \frac{(\gamma - 1)}{2} M_\infty^2\right]^{-1/2} + \frac{1}{K}\right) \cdot \frac{L}{D}} \tag{6}$$

It is possible to see that, for a fixed cavity geometry (i.e. fixed length-to-depth ratio) the Strouhal number for the fundamental acoustic loop frequency is only a function of freestream Mach number. This frequency is typically phase locked and is affected by a non-linear saturation phenomena, that conveys energy towards associated harmonics.

On the other hand, the low frequency values, responsible for the frequency modulation mechanism ([4],[7]), have their source in the internal flow, and more exactly from centrifugal instabilities in the recirculating eddies present in the cavity interior. Typical Strouhal numbers range from 0.005 to 0.05, depending from the source mechanism. Low Strouhal numbers are typically associated with velocity fluctuations in the layers of the recirculating flow inside the cavity, whereas higher modes are associated with the formation of sub-eddies inside the stratified layers of the main

[3] Unless otherwise stated, in this study the Strouhal number is calculating using cavity depth as reference length.

inner vortex. The interaction of these centrifugal instabilities with the acoustic modes of the shear layer occur due to non-linear quadratic coupling, as shown in previous studies ([5],[6],[8],[9]) and are responsible for the generation of the Rossiter-Heller tones.

Flow over a cavity has been a fundamental research topic and the influence of geometric parameters like length-to-depth/width-to-depth ratios has been consistently explored [10]. Nevertheless, the aero-acoustic response of a weapons bay can strongly differ from the standard rectangular cavity. Typical weapons bay aerodynamic and acoustic response is strongly influenced by external factors, such as local design solutions, which alter the reference rectangular shape ([11]–[18]). Dedicated studies evidenced the strong influence of bay doors on the cavity. Typically, the doors increase the overall acoustic signature and tonal response ([14], [19]–[21]). Another factor of pivotal importance is that in combat, military aircraft may operate the weapon bays at flight attitudes that typical experiments of "isolated" cavity do not account for. This is usually represented by non-zero angles of attack and sideslip, the effects of which on cavities have rarely been studied [22].

The present work seeks to expand previous studies on angle of attack effects on weapon bays, exploring the influence of this flow parameter in a geometry incorporating doors. Numerical analyses, at a transonic Mach number of 0.85 and supersonic Mach number of 1.20 were conducted on a rectangular cavity with leading and trailing edge serrations (typical of low-RCS airframes) and 90 degree open doors installed. Additionally, the force and moments induced on the doors by the unsteady flow-field were recorded, and their spectrum was compared with the doors' modal analysis to explore fluid/structure coupling.

II.Numerical Method - CFD

A. Cavity Geometry

The adopted cavity model was derived from the well-known M219 geometry, having a length-to-depth ratio of five and a width-to-depth ratio of one. The new geometry, shown in Fig. 1 introduced a double chevron step, of 5 mm depth, at the front and rear walls. The angle of the indentations was posed equal to 45 degrees, typical of the value present in military aircraft subjected to radar signature suppression/control design philosophies. The step height was chosen assuming the hypothesis that enough room would have been available to accommodate bay doors in their closed position ([23], [22]). The cavity was complemented by a set of 2 doors, opened at 90deg. The doors were separated, from the side surface of the cavity, by a gap of 1 mm.

The reference axis system for the cavity (X_c, Y_c, Z_c) had the origin coincident with the cavity leading edge, with the x-z plane coincident with the bay symmetry plane (see Fig. 1). On the other hand, the door axis system, in which accelerations were measured was centred at the door centre of gravity, as shown in Fig. 1. A single rake, consisting of 19 pressure probes was placed on the cavity floor to monitor pressure signals. The probe positions ranged from x/L=0.05 to x/L =0.95 and were evenly spaced.

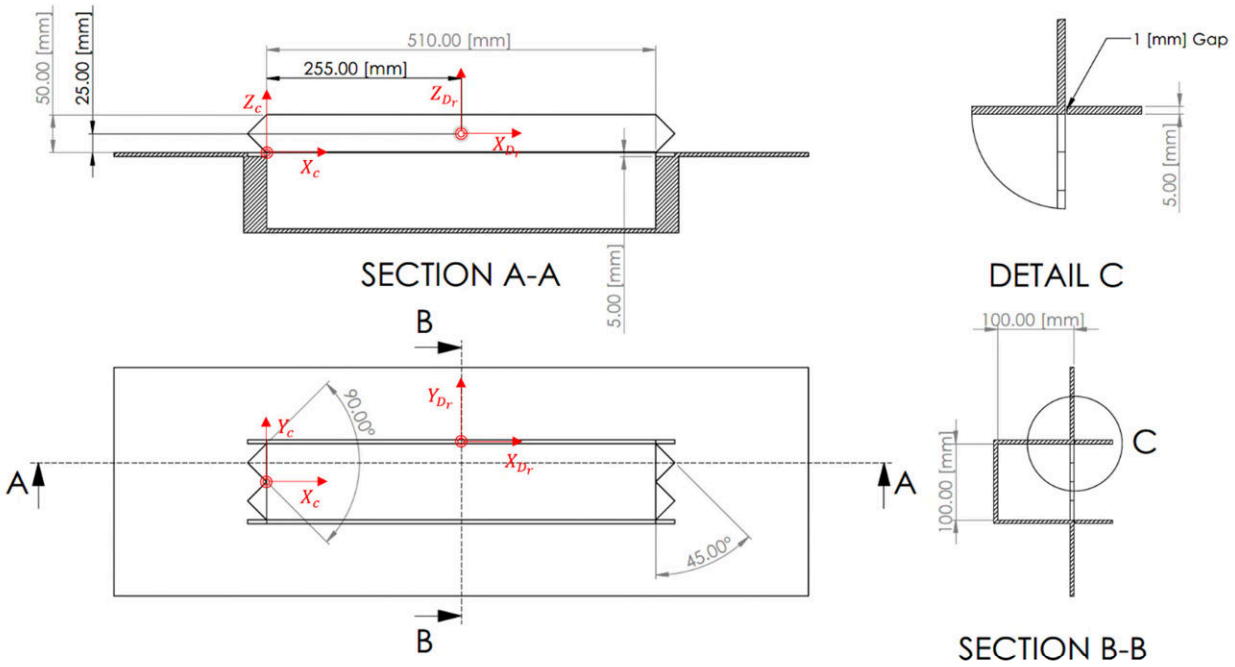

Fig. 1. Cavity geometry and axes definition.

Installing the cavity flush with one of the boundary faces of the computational domain would have not been suitable to explore angle of attack effects, as the upstream wall would have influenced the effective flow direction observed by cavity. Even if in practical applications (i.e. weapons bay) a surface is present upstream of the cavity leading edge, this has a longitudinal extension usually comparable with the cavity length, or less. Hence, for this study, it was decided to install the cavity on a support (see Fig. 2). Such an installation was considered a better representation to explore angle of attack effects on a weapons bay-like geometry.

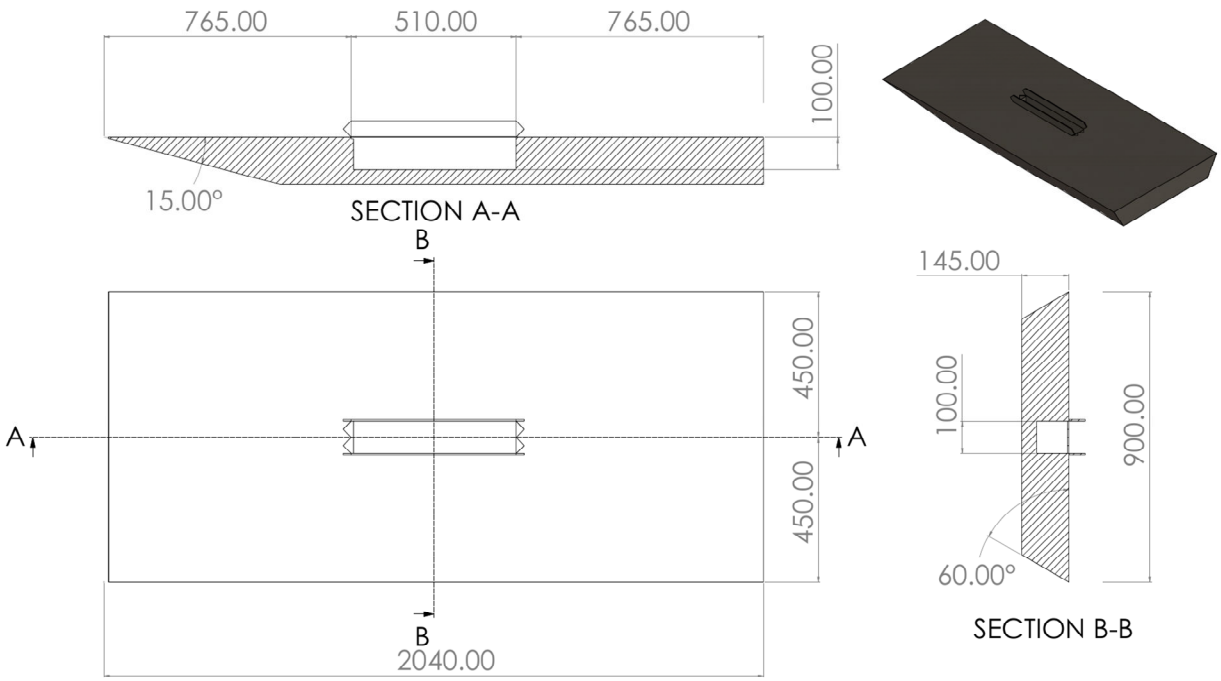

Fig. 2. Support geometry. Dimensions are in millimetres.

B. Numerical Simulation

The simulations in this study were performed using the SST-SAS turbulence model within the ANSYS Fluent 2021R2 CFD code. The capability of this code and the turbulence model to properly address cavity flow has been previously demonstrated by Egorov, et al. [24] .

An unstructured polyhedral-type mesh was used, with a prism layer wrapped around the viscous surfaces, for accurate boundary layer resolution, with a y^+ value of 1 or less. For accurate vortex structure modelling with SRS, the detached shear layer was resolved using a spacing equal to 0.05 times its minimum thickness (i.e. at the cavity leading edge), as suggested by Menter [25]. All solid walls were specified as adiabatic surfaces where the no-slip condition was applied. The computational outer boundary was specified as a far-field, using the modified Riemann invariants condition. The computational domain extended $6L$ to the right and left of support sides, $6L$ from the top and bottom limits of the support, and $8L$ upstream and $14L$ downstream from support leading and trailing edges respectively.

The air was treated as an ideal compressible gas using Sutherland's law for viscosity modelling. Due to the compressible nature of the problem a pressure-based coupled (in momentum and continuity) solver was used. Non-viscous fluxes were resolved using second order schemes; viscous fluxes were resolved using a second-order upwind scheme; gradients were evaluated using the least squares method. The time marching scheme was an implicit second-

order dual-time formulation. Five inner sub-iterations were found to be adequate, which is consistent with the recommendation of Menter [25] and the approach of Chaplin and Birch [26].

As advised by Menter [25], the time step was chosen to ensure a CFL number approximately equal to unity in the LES part of the domain. Unsteady simulations were initiated from a converged RANS solution to reduce the start-up time. To resolve accurately all the main features, the simulation was run for a total of 250 convective times (t_c), discarding the initial 100· t_c seconds to clear the solution from the start up transient. This allowed data sample lengths with temporal duration greater than 30 cycles of the lowest frequency mode of interest (1st Rossiter-Heller Mode) as in accordance with the values suggested by Menter [25].

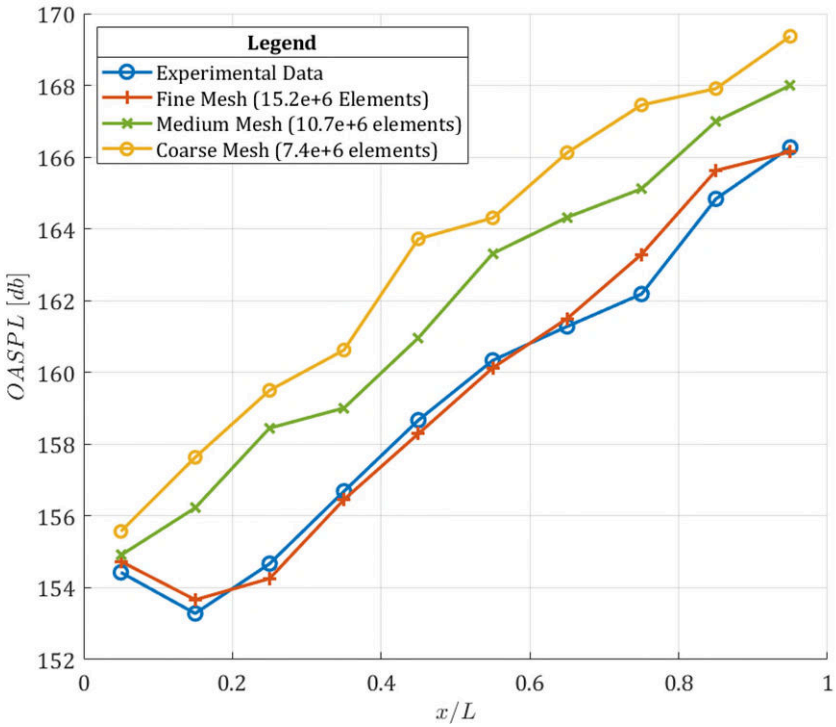

Fig. 3. CFD Grid convergence on OASPL, and comparison with experimental data [27]**.**

To validate the computational settings and mesh convergence, data were used from wind tunnel studies of the M219 cavity [27]. Three meshes, constructed around the M219 rectangular geometry, were developed (coarse, medium, and fine), and the results compared to the experimental data. Grid convergence was stopped when the numerical results showed a difference in the overall sound pressure level (OASPL) with respect to the wind-tunnel measurements at each of the ten measurement locations, of less than 2 dB (Fig. 3). This placed the numerical results within the error band of the experimental data [28]. The final mesh consisted of 15.2 million elements, of which 9.6

million were located inside the cavity. The presence of the doors changed the overall mesh count and for the final geometry (incorporating the doors, the transverse edge indentations, and the door gaps) the overall total was 22.4 million elements of which 11.2 million were located inside the cavity.

C. Test Matrix

The cavity was tested at two representative Mach numbers of the transonic and supersonic regime (0.85 and 1.20 respectively) . Angle of attack was considered positive with the z-velocity component in the cavity axis reference system (see Fig. 1) assuming negative values. Sideslip angle was fixed at zero. The following table summarise the test matrix with the boundary conditions:

Table 2 Test Matrix & Boundary Conditions

M_∞	$p_\infty\ [Pa]$	$T_\infty\ [K]$	$p_{0_\infty}\ [Pa]$	$T_{0_\infty}\ [K]$	$\alpha[deg]$	$\beta[deg]$
0.85	63177	266	101325	300	0.0	0.0
					2.0	
					4.0	
					6.0	
					8.0	
1.20	41784	233			0.0	
					2.0	
					4.0	
					6.0	
					8.0	

III.Numerical Method – Modal Analysis

The structural modal analysis was conducted only for the door geometry, as it was considered the most affected element in this configuration, and the loads are more affected by the flow.

A. Geometry

The door geometry used for the structural analysis was the same as for the CFD, but it was complemented by the introduction of five rectangular-bodies to represent the hinges, which in the simulation had the function of anchor points for the body (see Fig. 4). These cube-shaped additional parts, having 5 mm sides, and equally spaced across the door length were generated by comparing various weapons bay doors of existing combat aircraft. The idea was not to re-create an exact hinge model, but to introduce similar constraints in the geometry deformation.

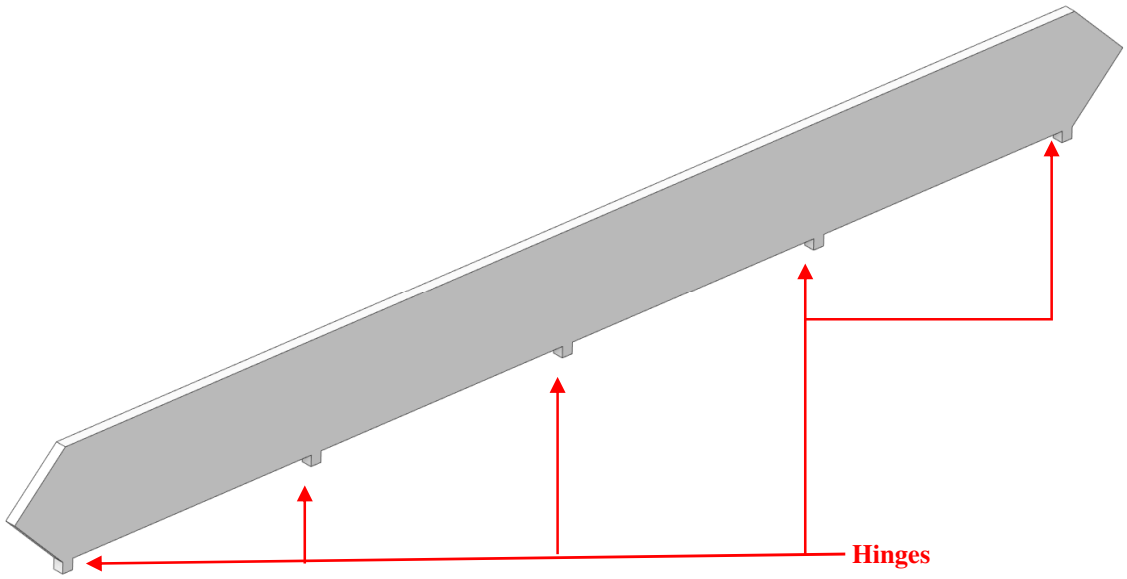

Fig. 4. Door model used in the structural modal analysis

Mass and inertia properties of the door are listed in Table 3.

Table 3 Door Mass and Inertia Properties

Property	*Value*	*Units*
m	0.3736	$[kg]$
I_{xx}	7.77e-5	$[kgm^2]$
I_{yy}	9.02e-3	$[kgm^2]$
I_{zz}	8.94e-3	$[kgm^2]$

B. Numerical Simulation

Modal analysis was conducted using ANSYS Mechanical ADPL 2021R2 code. The door body was discretised using hexahedral elements, imposing a minimum mesh size of 1 mm. This resulted in a total of 99000 elements, with the door thickness discretised with at least six nodes. A rigid contact boundary condition was placed at the bottom face of the hinges. The mode extraction method used the undamped approach. The material selected for this study was 2024 aluminium alloy. The number of modes extracted was iteratively increased until the cumulative effective mass fraction reached one for all six motion components ($u_x, u_y, u_z, \theta_x, \theta_y, \theta_z$) [29]. This corresponded to an extraction of 20 modes.

IV.Data Analysis Procedure

A. Flow Analysis

The mean flow analysis consisted in the study of the mean pressure coefficient $\overline{C_p}$ and the overall sound pressure level (OASPL), quantities respectively defined as:

$$\overline{C_p} = \langle \frac{2}{\gamma_{air} \cdot M_\infty} \cdot \left[\frac{p}{p_\infty} - 1 \right] \rangle \tag{7}$$

$$OASPL = 20\, log_{10} \left(\frac{\sigma_p}{p_{reference}} \right) \tag{8}$$

Here, the overbar indicates that the quantity has been time-averaged, whilst $p_{reference}$ is the minimum audible pressure, equal to 2 x 10^{-5} Pa, which is defined as the threshold of human hearing.

The non-stationary flow analysis was based on the study of the sound pressure level (SPL) of the fluctuating part of the pressure signals, which was defined as:

$$SPL(f) = 10\, log_{10} \left(\frac{PSD(f)}{p^2_{reference}} \right) \tag{9}$$

The power spectral density (PSD) was obtained using the Welch method [30], with the division of the original signal in smaller blocks of 50% overlap, and with a number of samples equal to the closest power of two of the ratio of f_s/f_r [4].

B. Bay Door Load Analysis

The door mean and unsteady loads generated by flow unsteadiness were reported in terms of acceleration and angular acceleration, in the door axis reference system (see Fig. 1). The relative spectra $a(f)$ and $\dot{\omega}(f)$ were calculated as follows:

$$a(f) = \frac{2|\hat{a}|}{N} \tag{10}$$

$$\dot{\omega}(f) = \frac{2|\hat{\dot{\omega}}|}{N} \tag{11}$$

[4] The frequency resolution was posed equal to 20 Hz.

Here $\hat{a}$ and $\hat{\omega}$ are the one-sided FFT of the acceleration and angular acceleration signals, whilst N is the number of samples of the time-series. This approach allowed the spectra to be expressed in units of $\frac{m}{s^2}/Hz^{1/2}$ and $\frac{rad}{s^2}/Hz^{1/2}$.

V.Results

A. Aero-Acoustic Analysis

1. Mean Flow Analysis

The evolution of $\overline{C_p}$ in the cavity's longitudinal dimension, at zero angle of attack, had a trend in line with the open-type one [10] at both Mach numbers. For the transonic case, in the front part of the bay up to x/L = 0.3, the curve had a negative gradient, with values ranging from -0.04 to -0.05. Passed this point the gradient's sign was reversed with $\overline{C_p}$ values increasing linearly up to a value of 0.08 at the rear of the cavity (Fig. 5).

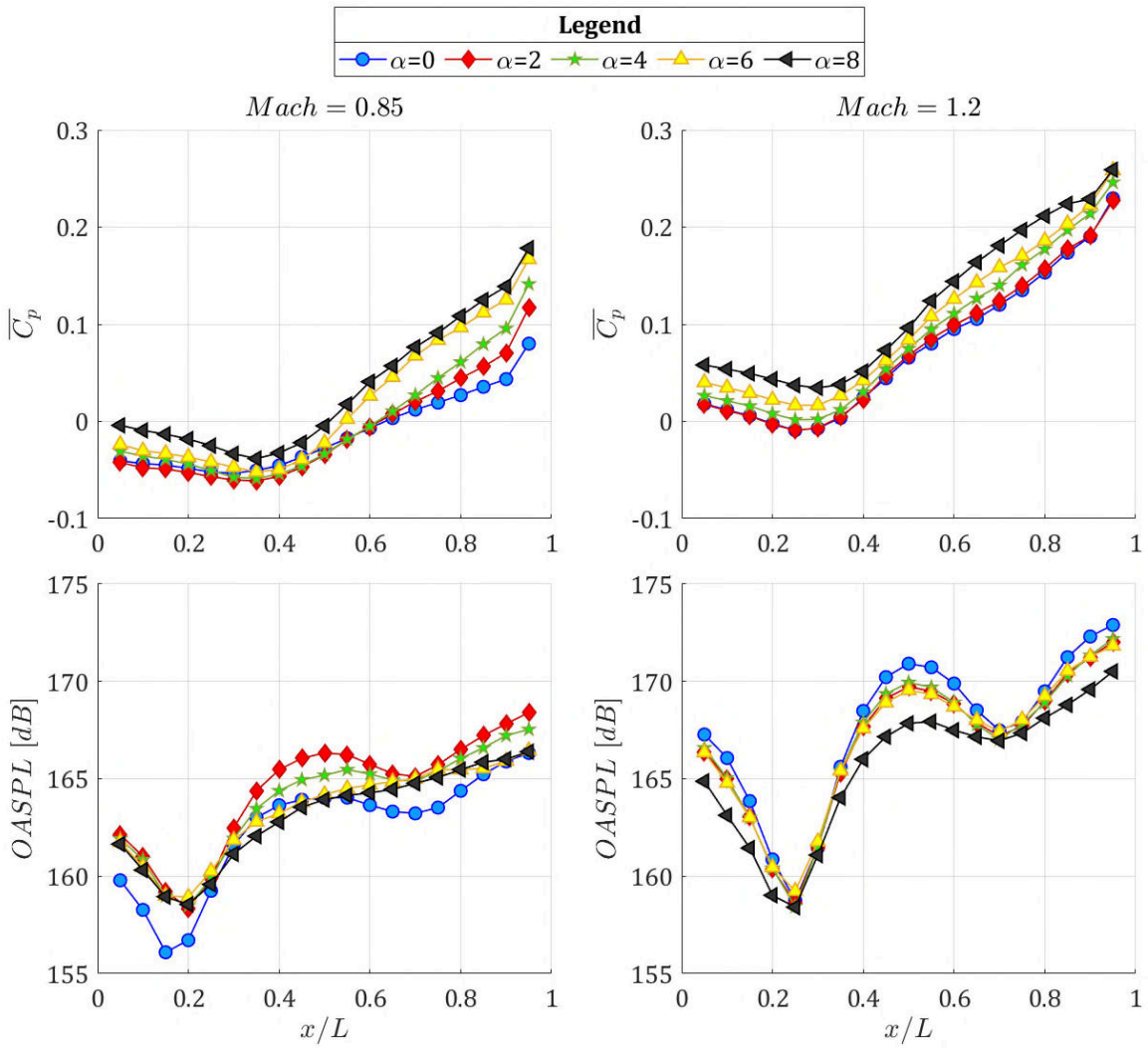

Fig. 5. Mean pressure coefficient and OASPL comparison. Left column, Mach=0.85. Right column, Mach=1.20.

On the other hand, whilst maintaining a similar-shaped curve, the supersonic case assumed higher values at all stations. In the front part, up to x/L = 0.3, values ranged from 0.018 up to -0.009, whilst the value reached at the rear wall was 0.23. When angle of attack was introduced it was observed that, whilst the qualitative trend of $\overline{C}_p$ remained unchanged, each increment of incidence progressively translated the curve towards higher values.

The analysis of the cumulative difference between each angle of attack increment step, was used to quantify this trend. Cumulative difference (d_k), expressed as a series, was defined as follow:

$$d_k = \sum_{i=2}^{k} (y_i - y_{i-1}) \qquad (12)$$

$$d_1 \equiv 0$$

$$y_i = \frac{1}{L} \int_{x=0}^{x=L} \overline{C}_p(x)_{\alpha=i} dx \qquad (13)$$

Here the quantity y_i is the rake-averaged value for the mean pressure coefficient at i^{th} angle of attack. This series was used to calculate how much the $\overline{C}_p$ value varied, with respect to the zero angle case, as angle of attack was increased. As show in Fig. 6 the trend was very similar for both Mach numbers, leading to the conclusion that the variations on mean pressure coefficient inside the cavity were directly correlated to the appearance of a vertical (i.e. directed along the cavity depth dimension) component of the freestream velocity vector.

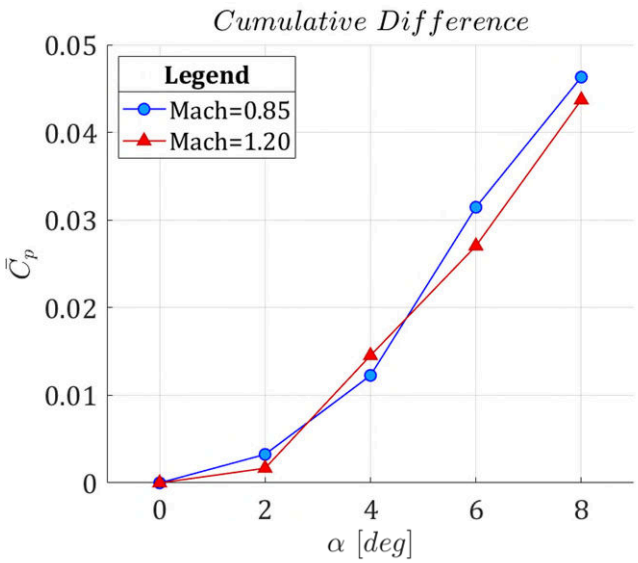

Fig. 6. Influence of angle of attack on the cumulative difference trend for the mean pressure coefficient averaged over the whole rake.

The influence of angle of attack on acoustic effects was also evident (Fig. 5), but the trend in this case was different between the transonic and the supersonic speed regime. At Mach 0.85, varying incidence from 0 deg to 2 deg caused an increase of 2 dB at stations between x/L = 0.05 to 0.2, and between x/L = 0.4 to 0.95. By contrast OASPL did not change between x/L = 0.25 and 0.35. Placing the cavity at higher angles of attack did not vary OASPL values in the front part of the cavity (up to x/L = 0.3). On the other hand, the rear and central part of the cavity experienced a progressive reduction of acoustic noise upon progressing towards higher angles of attack, up to the point where similar levels to the zero angle of attack case were attained. At supersonic Mach numbers the overall effect of angle of attack was to decrease progressively the acoustic noise, except for stations x/L = 0.25 and 0.7, where the OASPL values remained unchanged.

The line integral convolution (LIC) technique and OASPL contours were used to gain further insight on flow topology (Fig. 7 and Fig. 8). It was observed that at both transonic and supersonic Mach numbers, the interior of the cavity was dominated by a clockwise main vortex, which occupied up to 50% of the cavity volume. The centre of this main vortex did not change appreciably with angle of attack (Fig. 7 – symbol χ_ω). Such behavior was the direct cause of the invariance of the $\overline{C_p}$ curves' shape with angle of attack. Slices along the cavity symmetry plane (Fig. 7-Left) indicated a marked increase in high acoustic levels (orange/red contours) in the cavity centre and rear zones, upon increasing incidence to 2 deg. Further increase in angle of attack reversed the trend and the high-OASPL area began to shrink. This was accompanied by a reduction of the acoustic power emitted outside the cavity area (green-coloured contours). At supersonic Mach number (Fig. 7, right) the effects of angle of attack were different. In this case, the high-OASPL contour did not vary appreciably. Instead, it was the front shock, generated by the cavity leading edge, which experienced a dependence on incidence. The reference pattern, at $\alpha = 0$, consisted of a small (in terms of extension into the flow) normal shock, followed by a large oblique one. Upon increasing incidence, whilst the shape and size of the oblique shock remained unchanged, the front normal shock began to extend further into the flow, reaching a maximum extension at $\alpha = 4$. Passed this point, the normal shock shrunk to a size smaller compared to the case at zero angle of attack.

Flow effects on the area surrounding the cavity were analysed using a slice of the flow domain in correspondence with the cavity entry plane (Fig. 8). At transonic speeds, the major effect caused by increasing angle of attack was represented by the extension of the area, outside cavity perimeter, exposed to OASPL values higher than 150 dB (green and yellow coloured contours).

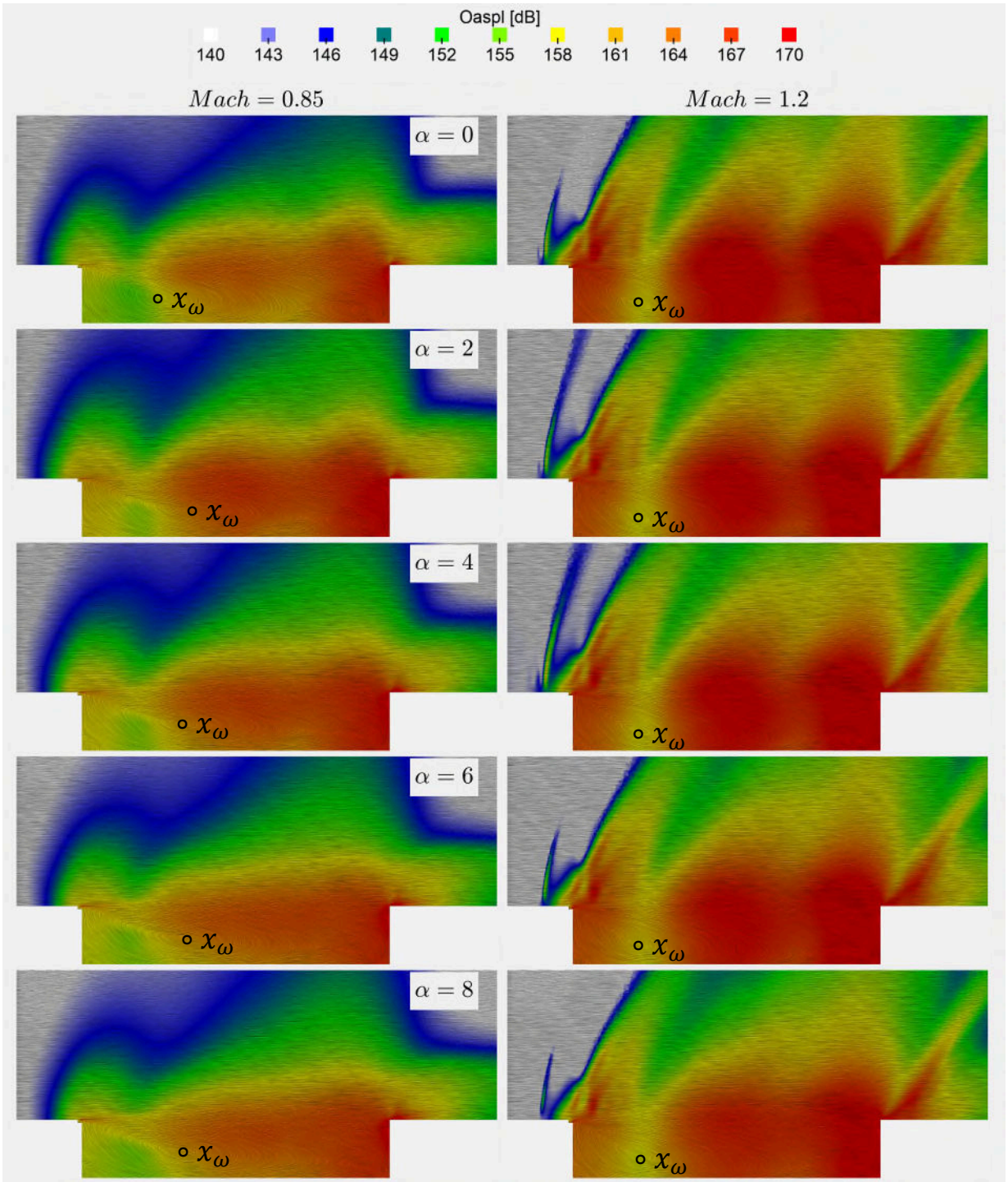

Fig. 7. Comparison of mean flow velocity LIC coloured by OASPL. Slice at $2y/W$ =0. Flow from left to right. Left column, angle of attack sweep at Mach 0.85. Right column, angle of attack sweep at Mach 1.20.

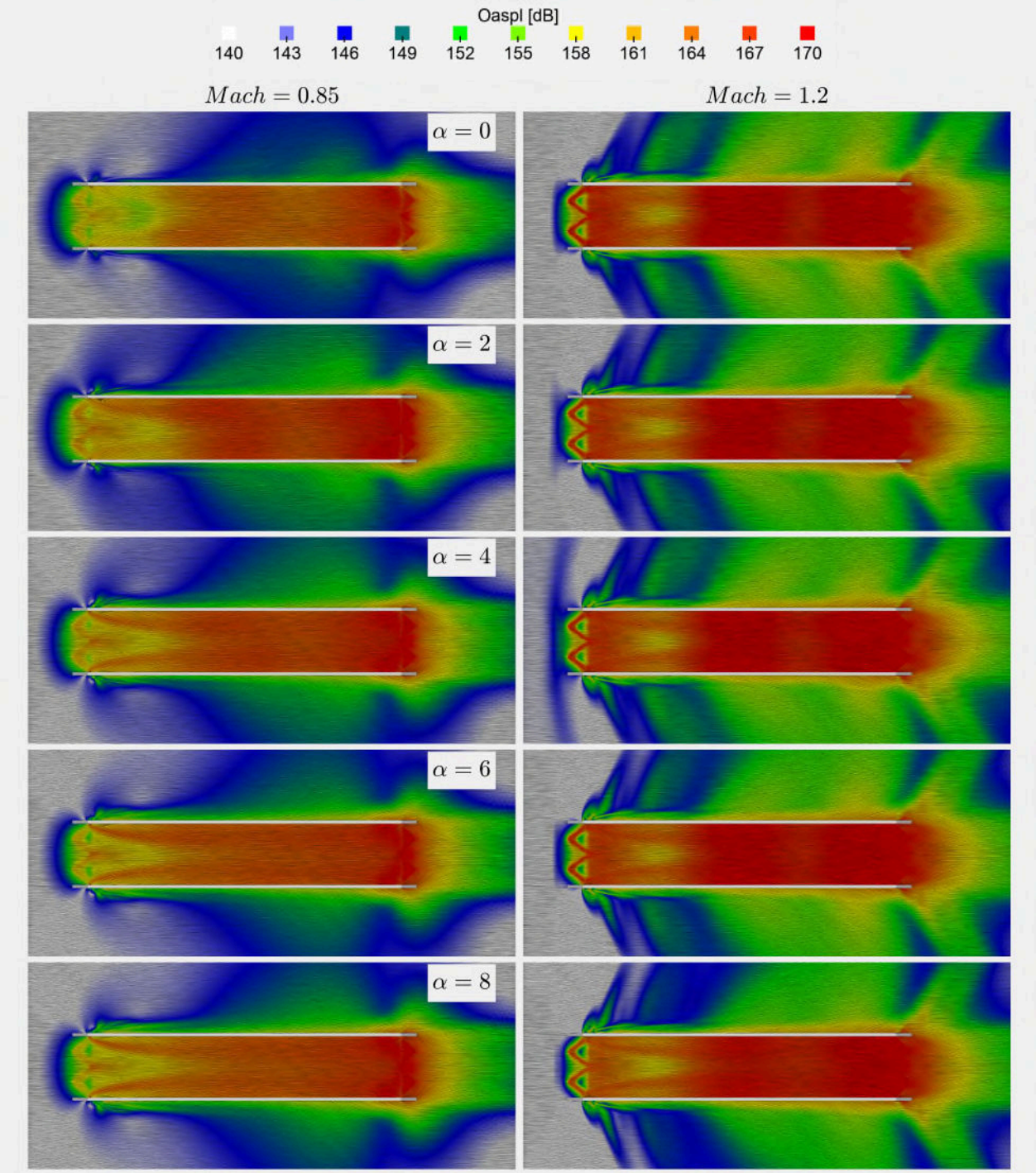

Fig. 8. Comparison of mean flow velocity LIC coloured by OASPL. Slice at z/D =0. Flow from left to right. Left column, angle of attack sweep at Mach 0.85. Right column, angle of attack sweep at Mach 1.20.

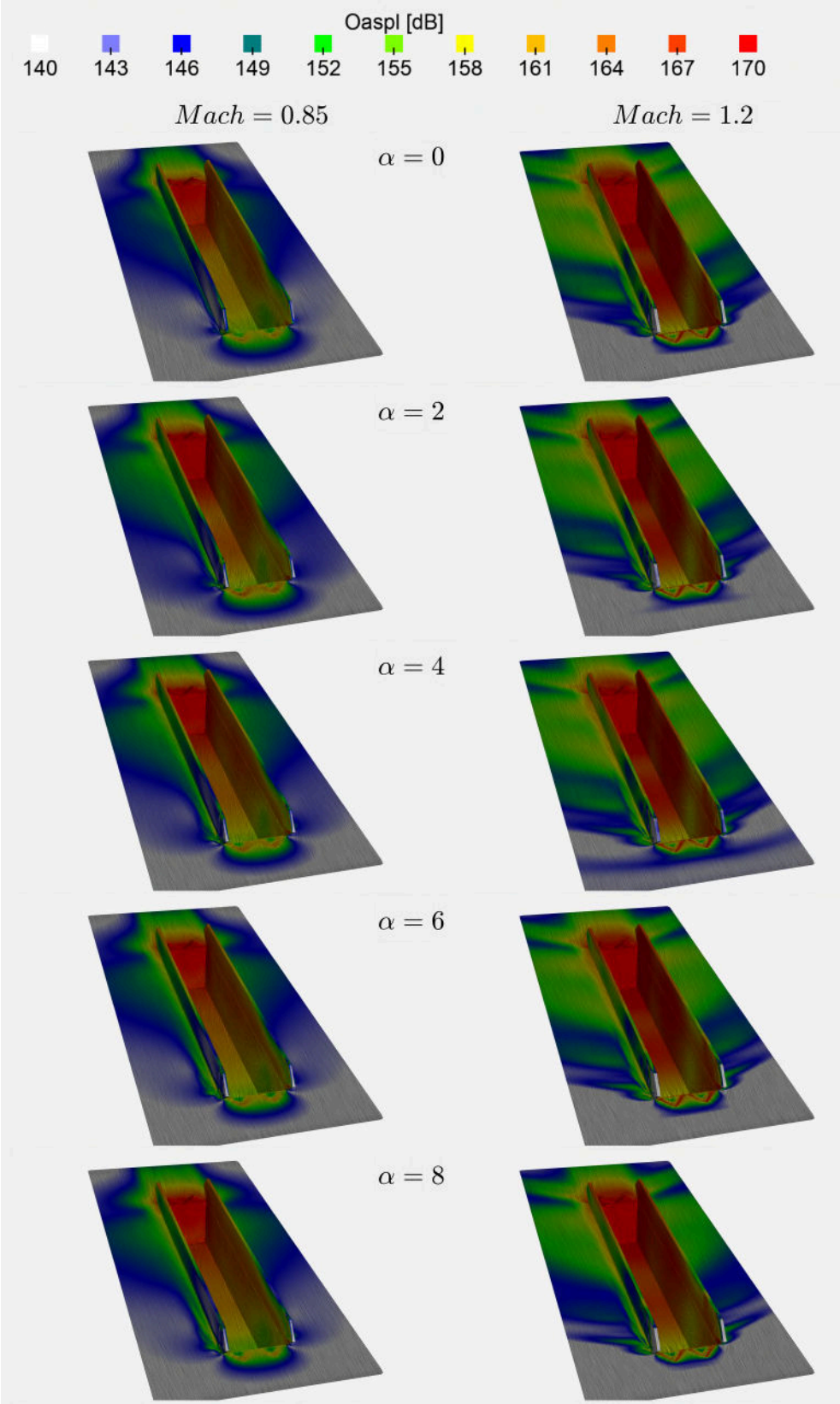

Fig. 9. Comparison of mean wall-shear LIC coloured by OASPL. Left column, angle of attack sweep at Mach 0.85. Right column, angle of attack sweep at Mach 1.20.

In the front part of the cavity, close to the door leading edge, the amount of flow spillage (moving from inside to the outside of cavity, through the door gap), and consequent associated acoustic load, increased constantly with angle of attack. Conversely, on the rear part, OASPL increased from $\alpha = 0$ to $\alpha = 2$ but reversed the trend if incidence was further increased.

The flow features at supersonic speeds were largely unaffected by angle of attack variations, except for the footprint of the normal shock at the cavity leading edge. Its extension/contraction reflected the pattern describe before.

To explore the acoustic load distribution on the cavity and door surfaces OASPL levels vs area distribution were plotted as shown in Fig. 10. The values were determined by calculating the area extension experiencing a determined range of OASPL values (for this study 20 levels were identified, ranging from 141 dB to 179 dB at intervals of 2 dB). The final area extension was then reported as the percentage of the total cavity (or doors) area. Hence, for example a value of 24% at 161 dB for the cavity, indicated that 24% of the cavity area experienced OASPLs between 160 dB and 162 dB.

As shown in the left column of Fig. 10, at transonic Mach number the shape of the curve was characterised by two peaks, one at 161 dB and the other at 157 dB. The former comprised nearly a quarter of the cavity area, whilst for the latter the value was 13%. Increasing angle of attack, up to 4 deg, minimally changed the values of these two peaks, but shifted their locations by 2 dB towards higher values. Further increases in angle of attack reduced the higher dB-peak area to 20% at $\alpha = 6$ and to 12% at $\alpha = 8$. On the other hand, the second peak moved towards lower values and incorporated more surface of the cavity. From a quantitative point of view, at zero angle of attack 61% of the cavity surface experienced an OASPL above 160 dB. This value increased up to 71% at $\alpha = 2$. Passed this point the cavity percentage area exposed to OASPL above 160 dB decreased linearly, reaching the final value of 63% at $\alpha = 8$. This was consistent with the flow visualisation of Fig. 7 and Fig. 9, where a progressive increase of low-OASPL area (green-coloured) in cavity's front part was observed. At supersonic Mach number, the shape of the curve changed showing only a dominant peak. In this situation, the angle of attack effect was minimal, and the percentage of area exposed to OASPL more than 160 dB remained constant at 90%. Again, flow visualisation (Fig. 7, Fig. 8, Fig. 9) indicated that OASPL inside the cavity was mainly independent to incidence variations. The overall picture was instead different when the doors were examined. In this case the distribution curve (Fig. 10) presented two distinct peaks at both transonic and supersonic speeds separated by an interval of more than 10 dB. This clearly reflected the different acoustic loading of the door between the side exposed to the cavity flow (inner) and the side exposed to

freestream flow (outer), as shown in Fig. 9. At Mach=0.85, the effect of angle of attack was observed on the door outer side-related peak, which moved slightly to higher OASPL values. On the other hand, the inner-side related peak was not affected by incidence variations.

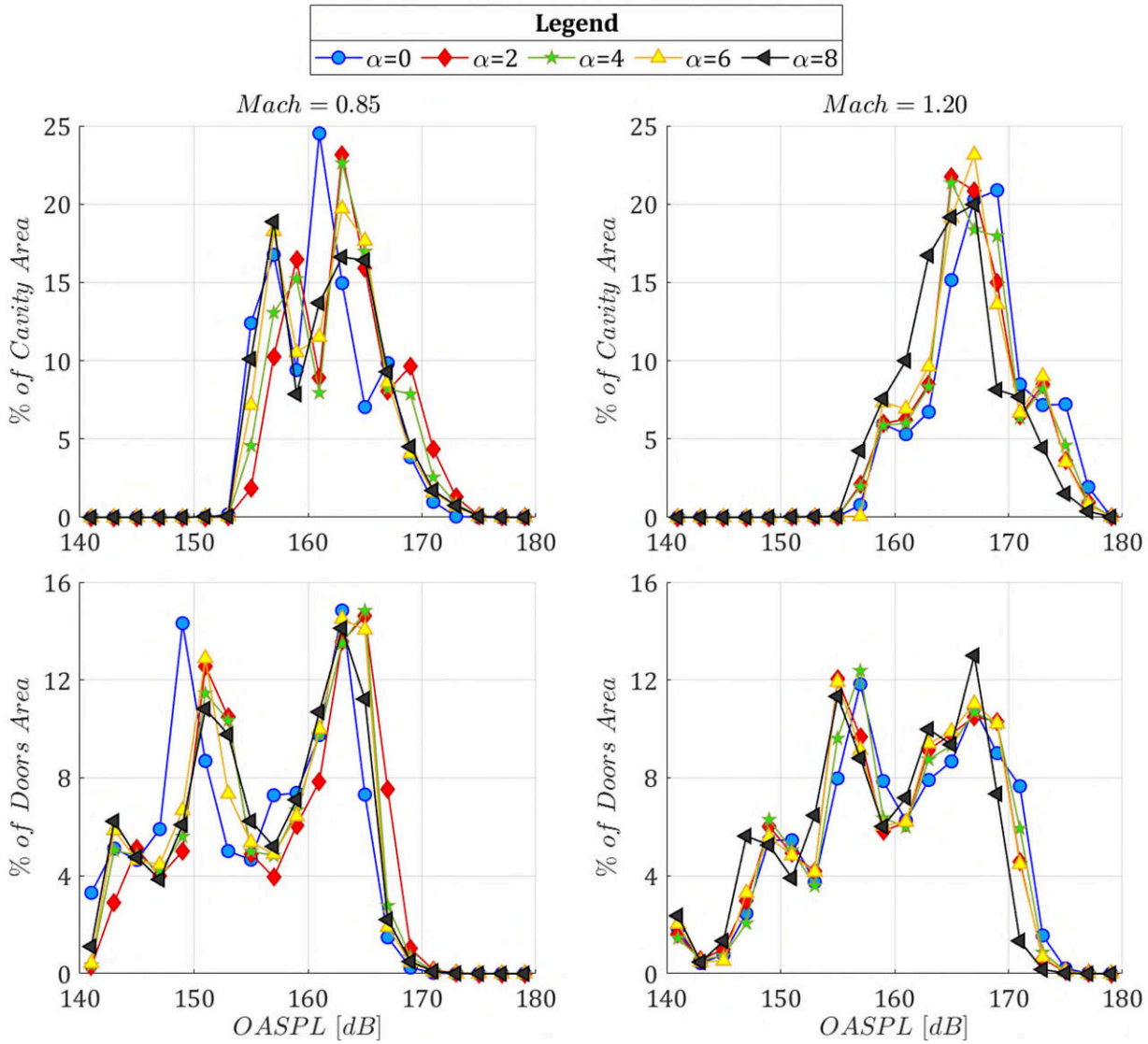

Fig. 10. Acoustic load distribution for cavity (upper row) and for doors (lower row) at different angles of attack. Left column, Mach 0.85. Right column, Mach 1.20.

At supersonic Mach number, the opposite was true, and in this case, it was the inner side of the door which experienced a marked increase in percentage of area at $\alpha = 8$. Regarding the percentage of the door surface exposed to OASPL levels more than 160 dB, the figures indicated that at Mach 0.85 and $\alpha = 0$, the corresponding value was 34%. Upon increasing incidence, this increased up to 45% at $\alpha = 2$, and then remained constant upon further increases

in angle of attack. At supersonic speeds 52% of the door area experienced OASPL values above 160 dB, and no variations on this value were observed upon increasing incidence.

2. *Unsteady Flow Analysis*

Spectral analysis conducted on the region of the cavity with the highest OASPL (probes at x/L=0.95) indicated that at Mach 0.85 three main tones, corresponding to Rossiter-Heller modes, were present as shown in Fig. 11. Whilst the theory predicted these values at 151 Hz, 364 Hz and 577 Hz, computational data located the modes at 146 Hz, 372 Hz and 549 Hz respectively. SPL levels indicated R_2 as being the dominant mode, with a value of 148.8 dB, whilst the R_1 and R_3 power was 144 dB and 143 dB respectively. Increasing incidence ($\alpha = 2$) slightly changed the peak locations in frequency. The resonant mode power did change; R_2 increased to 151.6 dB, R_1 increased to 141.7 dB, whilst R_3 dropped to 139.9 dB. Incidence effects were also observed on the background noise, which increased by 2 dB at frequencies above 1 kHz. Further increases in angle of attack (above 2 deg) reverted the trend, and all resonant modes experienced a drop in power attaining values lower than the zero angle of attack case. Additionally, at 4 deg and 6 deg R_1 was buried in the background noise and failed to appear. These findings reflected OASPL trends.

Moving to the supersonic regime, the spectra of pressure signal inside cavity were characterised by three resonant tones, corresponding to the 1st, 2nd, and 4th Rossiter-Heller modes. These were respectively R_1(144.2 dB, 219 Hz), R_2 (155.8 dB, 445 Hz), and R_4 (137.3 dB, 889 Hz). Within these, only R_2 was in line with the theoretically-predicted value, whilst the other modes consistently deviated from it. Increasing incidence did not change the frequency of the resonating tones but reduced the peak power of R_2 and R_4, again in line with the outcomes of OASPL analysis. The SPL value of R_1 did not change appreciably.

The application of Delprat's decomposition showed that the main parameters were not in line with the theoretically-predicted values. At zero angle of attack, and transonic Mach number, the main feedback loop frequency f_a was 201 Hz, whilst the modulation parameter ξ was 0.235. By comparison the predicted values were respectively 212 Hz and 0.289. The effect of angle of attack was observed on both f_a and f_b, as shown in Fig. 12. Here the feedback-loop frequency and the main modulation frequency varied with incidence but it whilst the changes in f_a with angle of attack were in the order of 5%, the variations of f_b were higher at up to 25%. At supersonic speeds, the situation was different. The maximum observed variation of f_a respect to the $\alpha = 0$ case was still around 5%, whilst the value for f_b rose to 4 times the original computed parameter at an incidence of 4 deg.

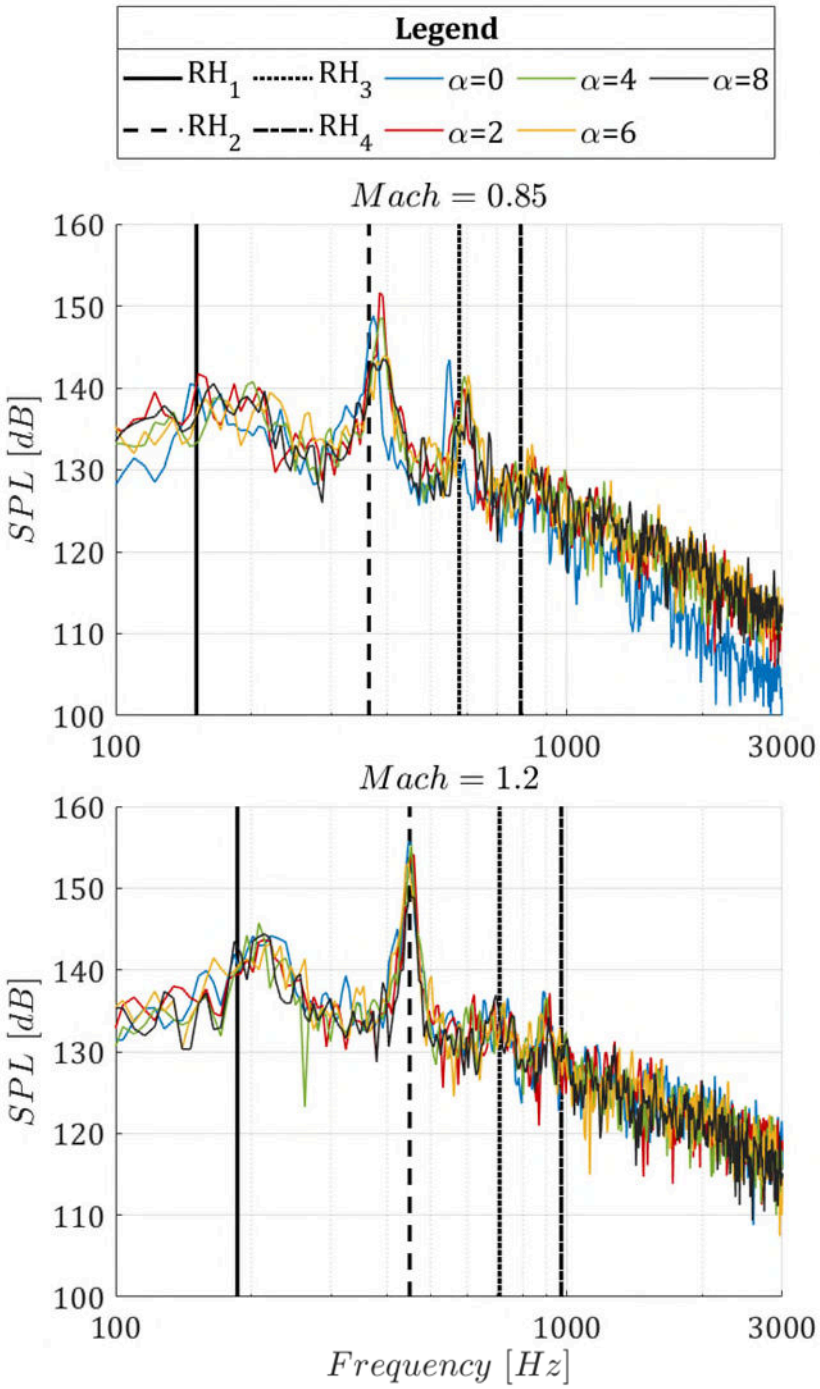

Fig. 11. SPL comparison for probe located at x/L=0.95, $2y/W$=0.00, z/D=1.00. Upper figure, Mach 0.85. Lower figure, Mach 1.20. Black-coloured vertical lines represent Rossiter-Heller predicted modes.

It is proposed that the observed effect of angle of attack on Delprat's parameters was because of the inflow component of the velocity vector correlated to angle of attack. This influenced the evolution of the main recirculatory vortex, and then its instabilities (directly correlated to f_b), and the shear layer trajectory (responsible for the feedback loop f_a). Previous studies [9] indicated that these phenomena are strongly non-linear, and minimal external influences

could have been the cause of the high sensitivity of the associated central frequencies to even minimal local flow changes. The findings of this study are in line with previous works on the effect of incidence on weapons bay aero-acoustic response [22]. Previous studies also showed the existence of a critical angle of attack, up to which the acoustic response increased, and after which, both OASPL and SPL decreased coherently with increasing incidence. Nevertheless, whilst in previous studies a consistent trend of Delprat's parameters with angle of attack was observed, in this case such consistency was not present.

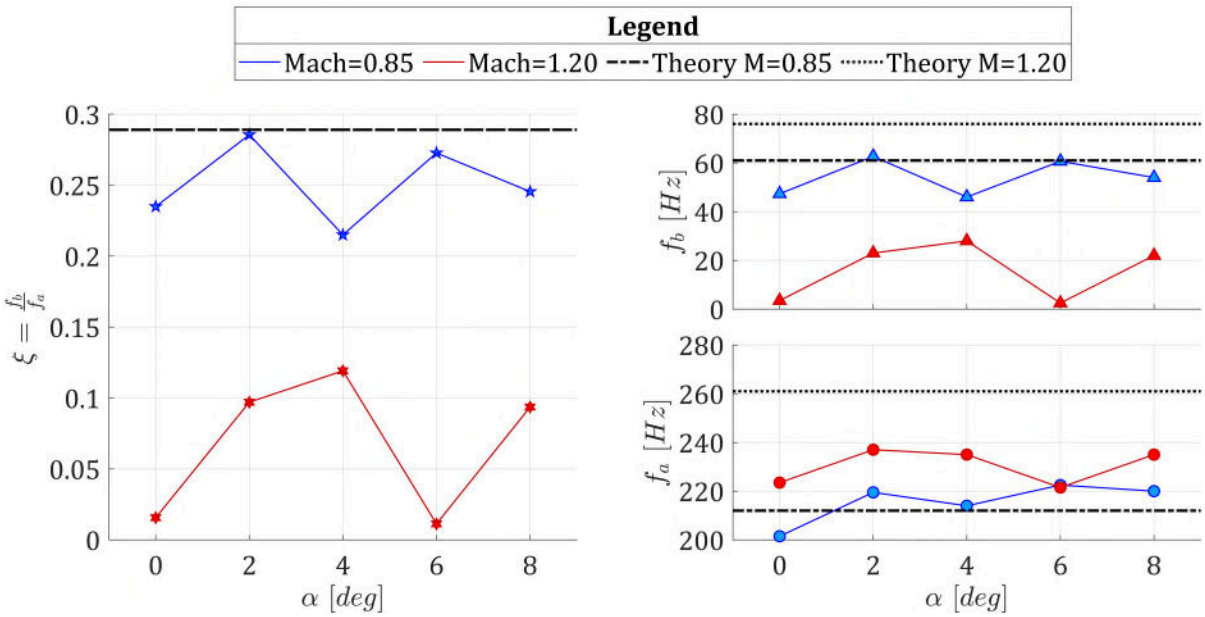

Fig. 12. Angle of attack and Mach number effects on Delprat's decomposition parameters.

B. Modal Analysis

A total of 20 modes were extracted during the structural analysis. Nevertheless, just four were considered fundamental, as they accounted for more than 75% of the effective total mass in all principal directions of deformation. These were M_1 (385 Hz), M_2(487 Hz), M_9(1840 Hz), and M_{15} (3885 Hz). The associated displacements are shown in Fig. 13.

Table 4 Summary of Principal Modes Characteristics for the hinged door.

Mode	f *[Hz]*	*Ratio of Effective Mass to Total Mass %*					
		u_x	u_y	u_z	θ_x	θ_y	θ_z
M_1	385	-	75.05	-	99.11	-	54.86
M_2	487	-	-	-	-	-	20.25
M_9	1840	-	10.62	-	-	-	-
M_{15}	3885	98.87	-	-	-	-	-
	Total	**98.87**	**85.67**	**-**	**99.11**	**-**	**75.11**

M_1 comprised a flexural response along the door's y-axis coupled with torsional deformation along the x-axis and z-axis. M_2 was related to the torsional deformation of the structure in the z-axis direction. The difference between M_1 and M_2, regarding the deformation around the z-axis, was that M_2 had a nodal point whilst M_1 did not. M_9, still involving flexural response along the y-axis, differed from M_1 as the former contained multiple nodal points, coincident with the hinges. Finally, M_{15} represented shear deformation along the x-axis. Table 5 summarises these principal modes with their relative contribution to the total mass for each direction. It was noteworthy that no appreciable contribution was observed for u_z and θ_y. This outcome was, nevertheless, expected as these deformation directions were directly blocked by the no displacement constraint imposed on the base of the hinges.

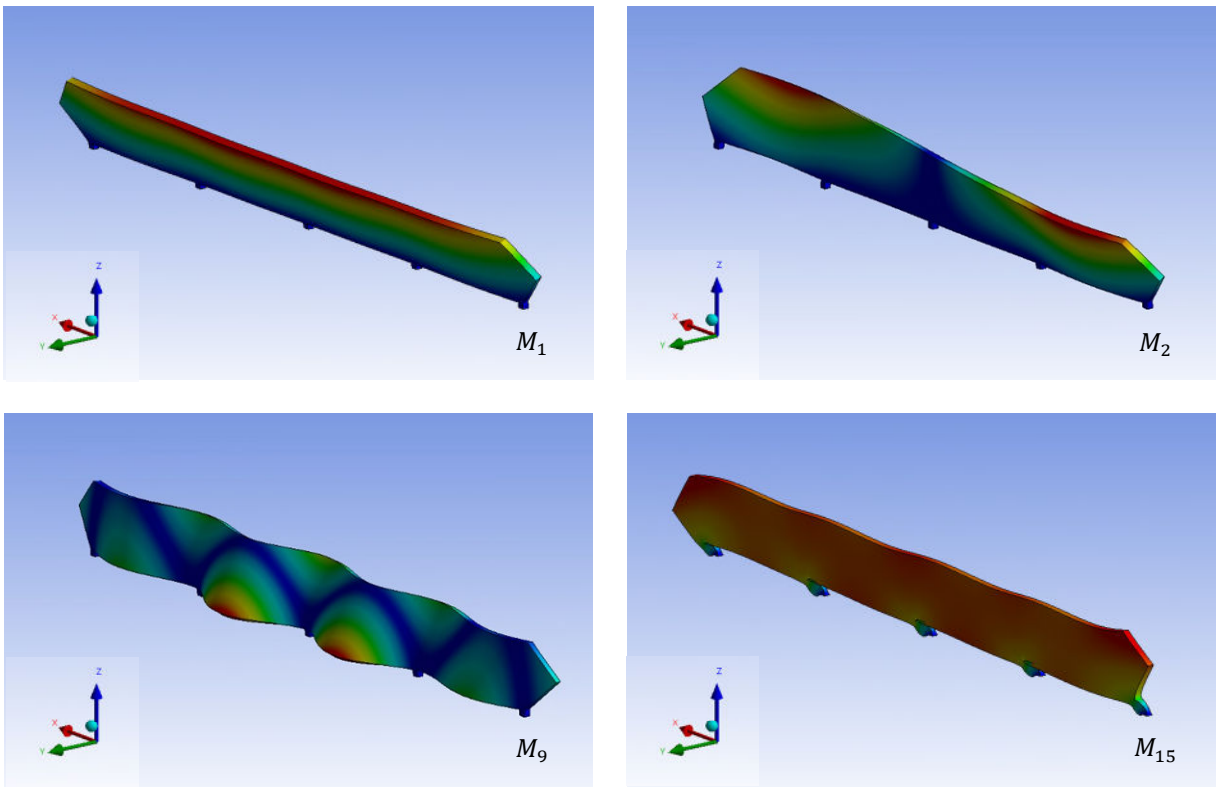

Fig. 13. Principal structural modes visual identification. Contours coloured by non-dimensional deformation (ratio of local nodal displacement to maximum nodal displacement)

C. Door Load Analysis

Door effects were reported in terms of linear and angular accelerations. Again, the analysis was divided between mean values (and the relative rms trends) and the associated spectra.

Analysis of the mean values of linear accelerations indicated a predominance in the y-direction (Fig. 14-Upper left). It was also observed that, whilst at a transonic speed, the x-component and the y-component were similar, but at

a supersonic Mach number, this was not the case, with μ_{a_y} attaining a value twice as big as μ_{a_x}. On the other hand, the linear acceleration along the z-direction was an order of magnitude smaller than the other components at both velocities. Angle of attack influence was only observed on the y-component which linearly increased at both transonic and supersonic Mach numbers. By contrast, incidence had no effect on the x and z components. The analysis of the rms values (Fig. 14-Lower left) showed a strong unsteadiness in time of the y-component. In this case angle of attack influence was negligible.

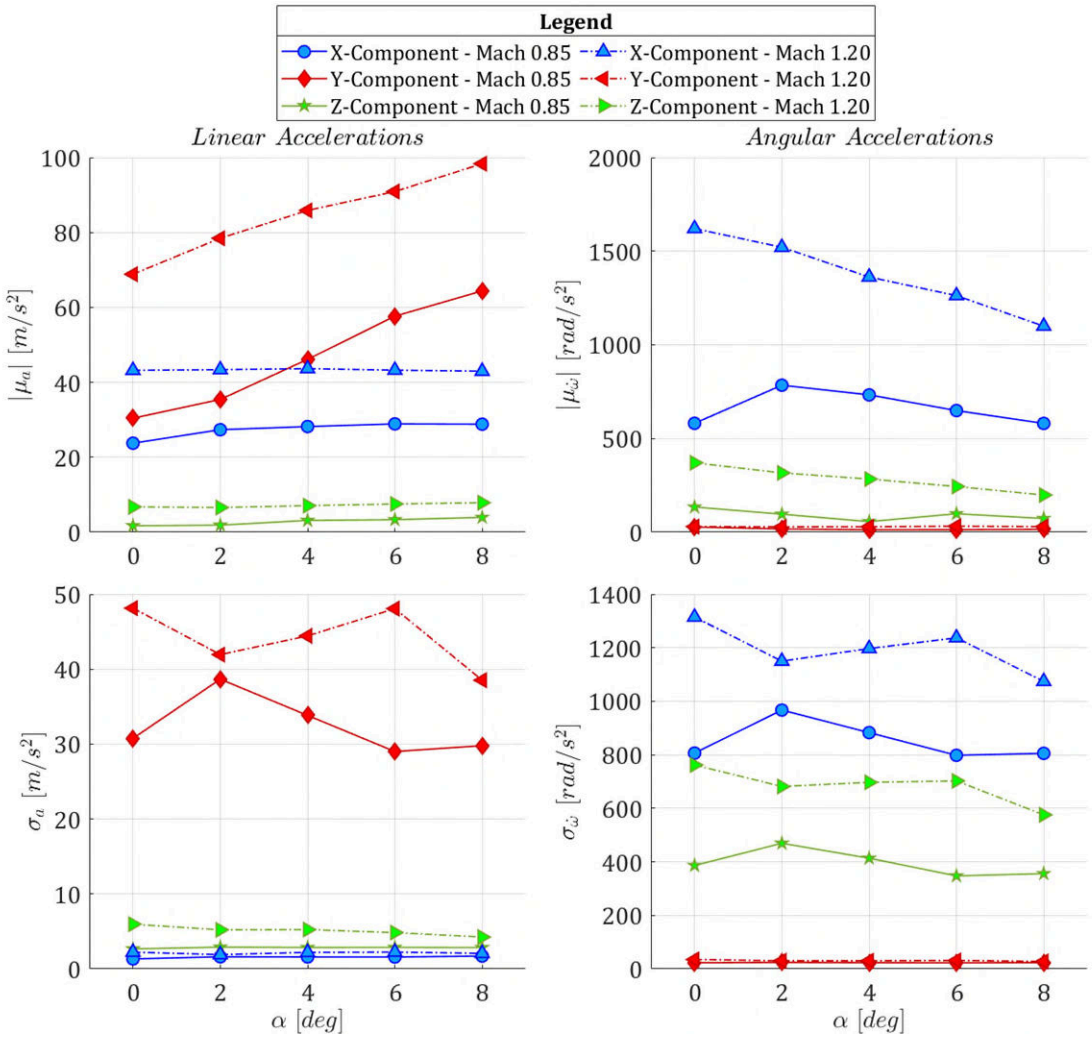

Fig. 14. Angle of attack effects on mean and rms absolute values of angular and linear accelerations components relative to bay doors.

Regarding angular accelerations, the x component was the dominant for both mean and rms values (Fig. 14-Upper and lower right). The z-component was the second in order of magnitude and attained high rms values as well. The overall effect of incidence was to decrease the magnitude of both mean and rms values. These findings indicated that

the main effect of the flow was a tendency to push the doors open or closed, whilst the drag effect along flow direction was of secondary order.

Spectral analysis of accelerations was separated by components and summarised in Fig. 15, 17, and 18. In all cases, peaks were observed in induced accelerations which were compared to the modal analysis results. In the x-direction, the critical frequencies were represented by M_1(385 Hz) and M_{15} (3885), accounting for 99% of participation factor, respectively for rotation and translation. The spectrum of x-linear accelerations (Fig. 15-Upper) showed low-power spectra, with resonant peaks located in the band between 150 Hz to 900 Hz, away from the critical value of M_{15}, hence not constituting potential problems in terms of fluid-structure interaction.

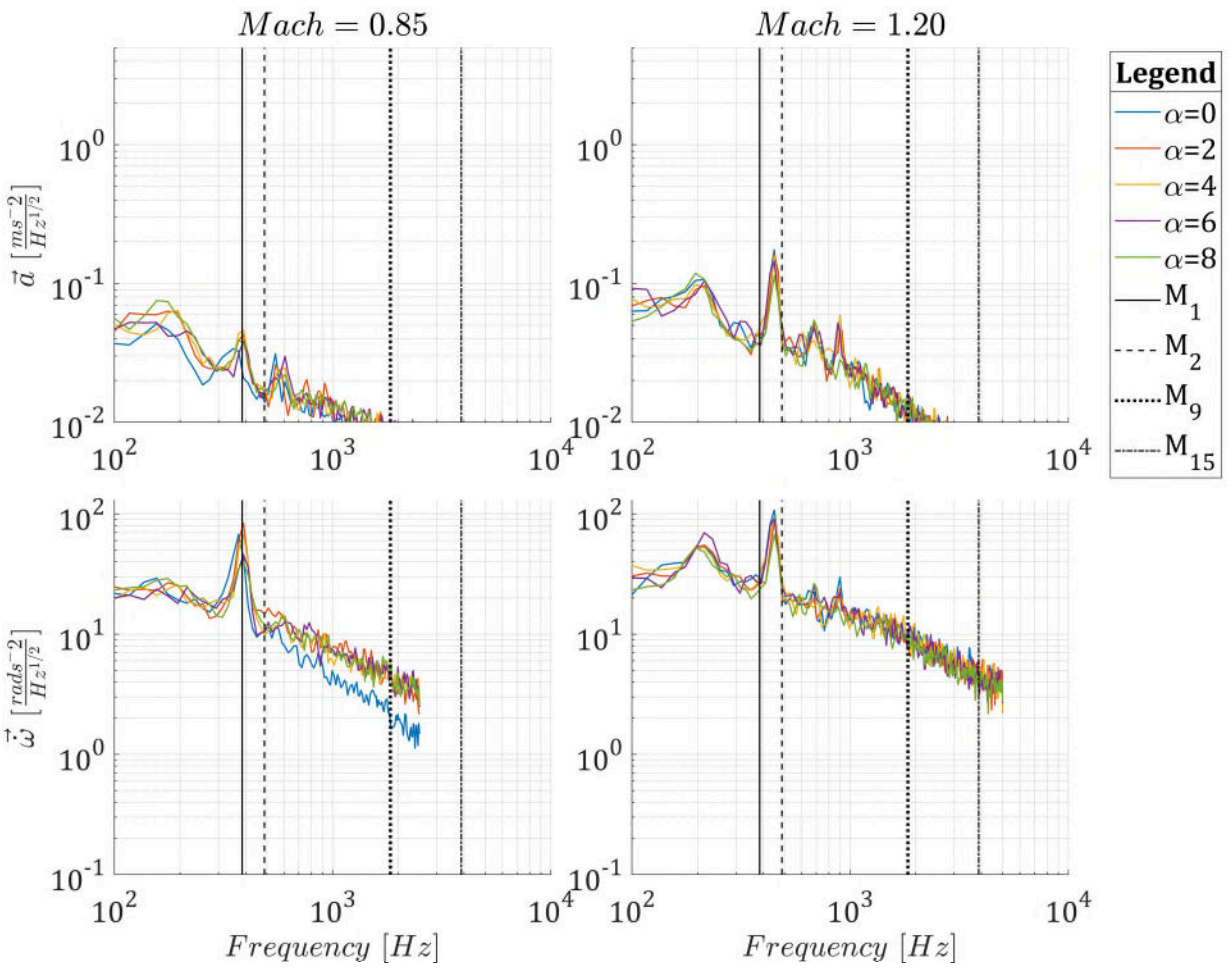

Fig. 15. Angle of attack effects on spectra of angular and linear accelerations relative to bay doors. X-component.

By contrast, the spectrum of angular accelerations at Mach=0.85 (Fig. 15-Lower left), showed the presence of a high power peak, corresponding with the critical frequency M_1. If the speed was increased to the supersonic regime, the main peak moved to higher frequencies (~450 Hz), and a secondary tone appeared centred at 215 Hz. The overall

effect of angle of attack was different between the two Mach numbers regimes. At Mach 0.85, for α =2, there was an increase in the overall power of 30%, with respect to the zero incidence case. However, further increasing incidence, progressively reduced it, with a final power, at $\alpha = 8$, 40% lower than $\alpha = 0$. This trend closely reflected that of the pressure signals discussed in the previous section. At Mach 1.20, the main peak experienced a constant decrease in power with angle of attack, whilst the secondary one remained nearly unaffected except for the $\alpha = 6$ case, which represented the highest value attained by this tone.

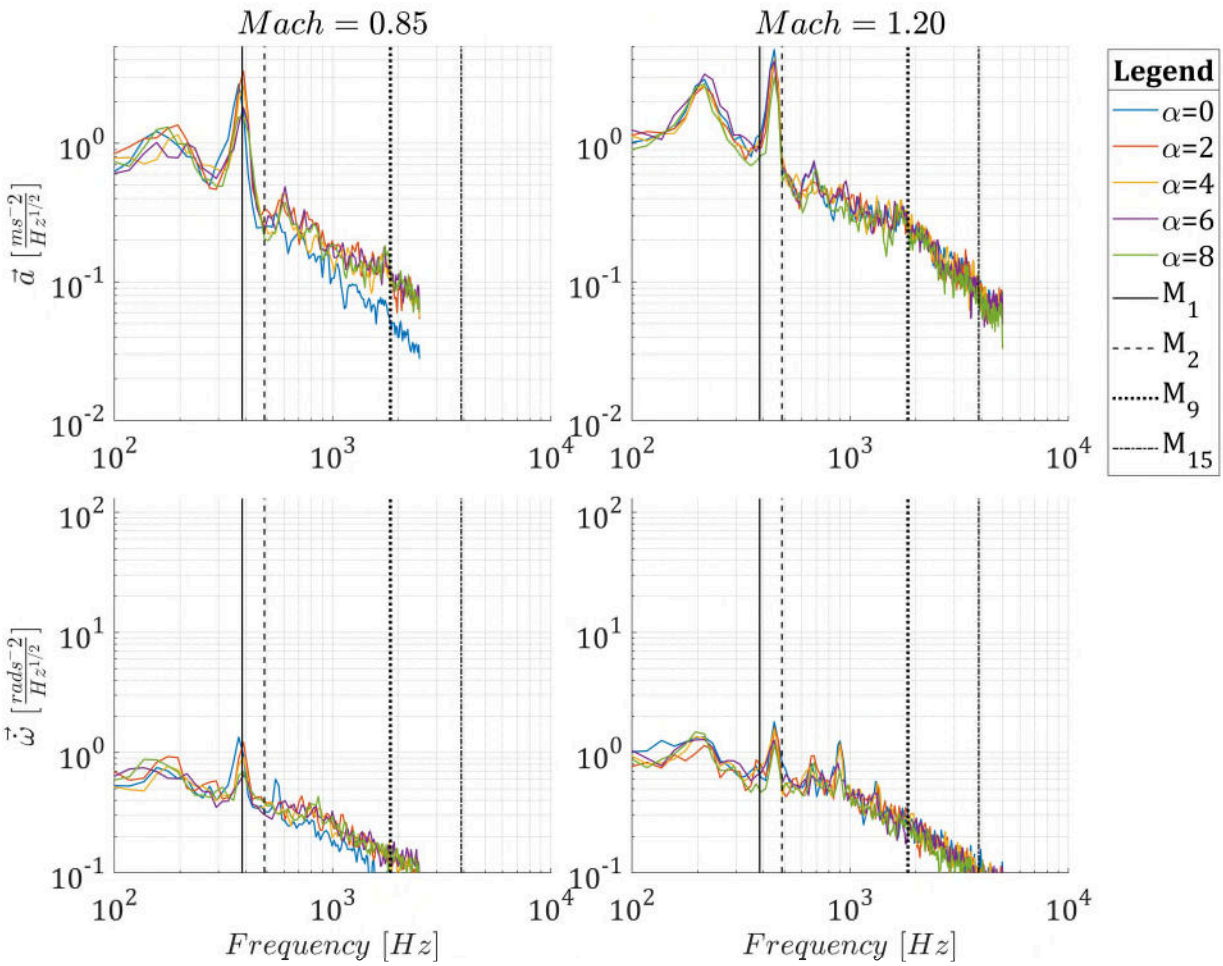

Fig. 17. Angle of attack effects on spectra of angular and linear accelerations relative to bay doors. Y-component.

In the y-component analysis, the key modes were M_1(385 Hz) and M_9(1840 Hz). Here the response of angular acceleration (Fig 17-Lower) attained power levels an order of magnitude smaller than the x and z ones, and hence was considered negligible. On the other hand, the linear acceleration in the y-direction was the most prominent. Fourier analysis (Fig. 17-Upper) showed that at Mach 0.85 a peak was present, corresponding to M_1. This was accompanied

by a secondary one at 195 Hz. Similar, to the x-component case, the trend with angle of attack was an initial increment in power up to $\alpha = 2$, followed by a constant decrease moving to higher incidences. At Mach 1.20 the main peak moved toward higher frequencies (~450 Hz), whilst the secondary one appeared, centred at 214 Hz, having a power similar to the dominant tone.

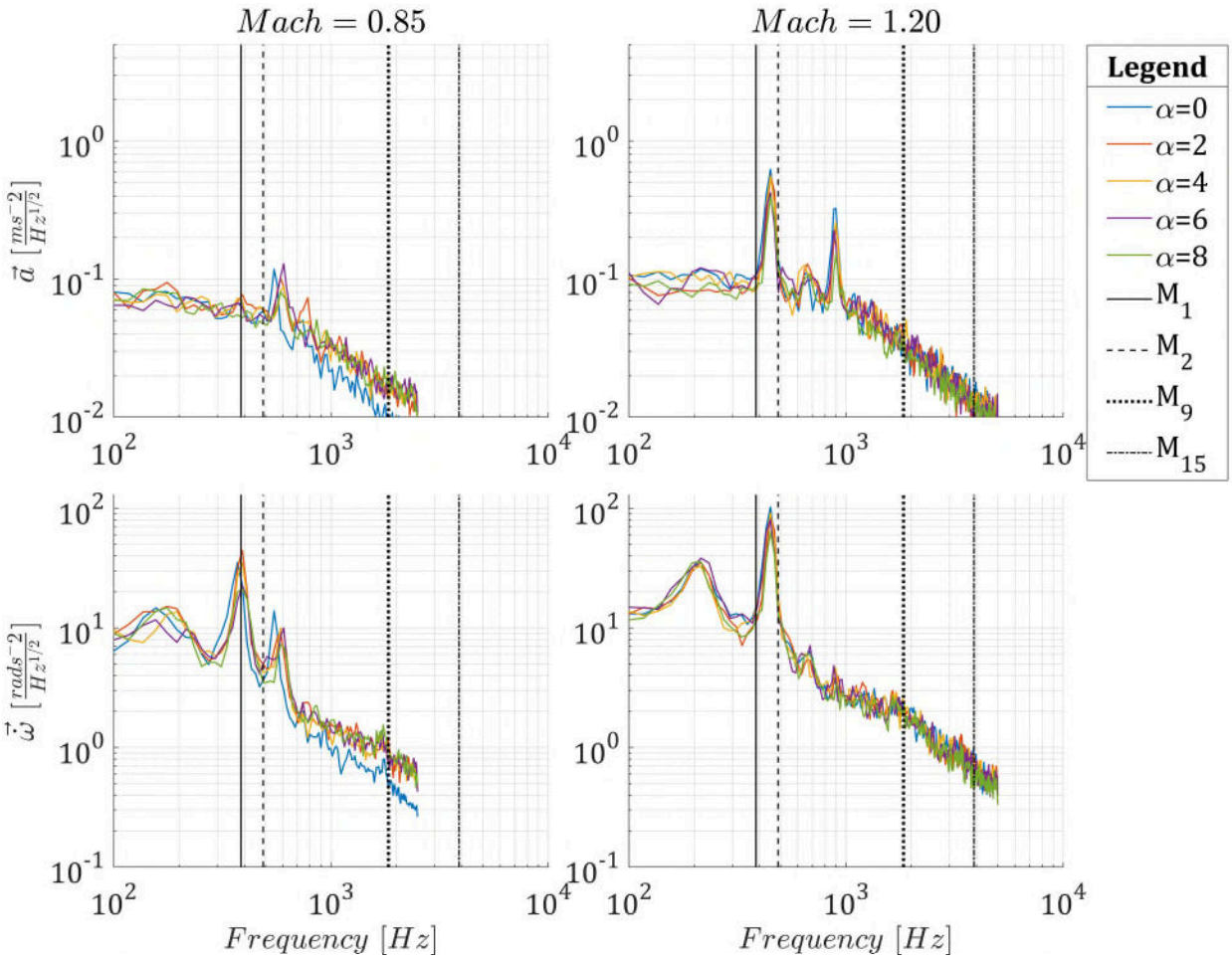

Fig. 168. Angle of attack effects on spectra of angular and linear accelerations relative to bay doors. Z-component.

Finally, the z-direction modes were related to M_1(385 Hz) and M_2(487 Hz) accounting for 55% and 20% of the rotation around this direction respectively. The door linear acceleration spectra (Fig. 18-Upper) were of low power in the transonic case, but at Mach 1.20 two high-power peaks appeared at 450 Hz and 898 Hz. Nevertheless, these were considered of secondary importance as the doors did not present displacement modes in the z-direction. Conversely, angular accelerations indicated that potential fluid-structure interactions were likely to occur at both Mach numbers (Fig. 18-Lower). At transonic speed a major peak was again observed corresponding to M_1, with a secondary one

relatively close to M_2 at 550 Hz. At supersonic speed the major tone occurred at 450 Hz, indicating a potential coupling with M_2. As in the case of the x and y components, in this Mach regime a second peak was present at 214 Hz.

The overall analysis of the spectral signature on linear and angular accelerations acting on the doors indicated that the possibility of fluid-acoustic coupling was likely to occur as all spectra showed a predominant tone located at the same frequency as the first structural mode M_1. This mode was characterised by having almost entirely the structure effective mass for displacements along the y-direction, and rotations around the x and z-axes. As linear acceleration was dominated by the a_y component and angular acceleration by the $\dot{\omega}_x$ and $\dot{\omega}_z$ components, aerodynamic-induced structural resonance was likely to occur.

VI.Conclusion

The study explored the influence of angle of attack, in the acoustic response and the induced forces on the doors related to a representative model of a low-RCS weapon bay at transonic and supersonic regimes.

The overall incidence effect varied according to the speed regime at which the cavity was exposed. At a transonic Mach number, it was shown that the existence of a critical value for angle of attack, between 2 deg to 4 deg, up to which the OASPL and SPL response of cavity increased. Beyond this point the acoustic response decreased with incidence. Flow analysis indicated that the angle of attack correlated with a minor change in position and configuration of the cavity's main recirculatory vortex.

At supersonic speed this trend was confirmed qualitatively, but the effects were minor, and in some parts of the cavity, OASPL values did not change with incidence variations. Inspection of the OASPL contours showed that the main effect of angle of attack on the flow configuration was on the bay's leading shock wave, which changed in shape even with minor variations in incidence. The overall conclusion was that the acoustic response of the cavity was mainly dependant on Mach number. Incidence variations induced local flow modifications which slightly altered the response quantitatively but not qualitatively.

The analysis of disturbances induced by the flow on the door structure indicated that the major contribution was correlated with the linear acceleration in the y-direction and angular accelerations in the x and z-directions. Angle of attack variations had secondary-importance in the unsteady part of the accelerations. Here modal analysis indicated that a potential fluid-structure resonance was possible as the main door mode coincided with the strongest peak in the acceleration spectra.

On the other hand, it was observed that the most prominent influence of angle of attack for this study was observed in the analysis of the mean values of the strongest components of acceleration, which were in the y-direction for the linear case, and in the x-direction for the angular case. In fact, the former nearly increased by 100% moving from $\alpha = 0$ to $\alpha = 8$ at both Mach numbers. Instead, the mean value for the x-component of angular acceleration, whilst being nearly insensitive to incidence variations in the transonic regime, at supersonic Mach number decreased by up to 25% when angle of attack was increased to 8 deg.

VII.References

[1] D. Rockwell and E. Naudascher, "Review—Self-Sustaining Oscillations of Flow Past Cavities," *Journal of Fluids Engineering*, vol. 100, no. 2, pp. 152–165, 1978, doi: 10.1115/1.3448624.

[2] J. E. (Royal A. E. R. Rossiter, "Wind Tunnel Experiments on the Flow Over Rectangular Cavities at Subsonic and Transonic Speeds," London, 1964.

[3] H. H. Heller, D. G. Holmes, and E. E. Covert, "Flow-induced pressure oscillations in shallow cavities," *Journal of Sound and Vibration*, vol. 18, no. 4, pp. 545–553, Oct. 1971, doi: 10.1016/0022-460X(71)90105-2.

[4] N. Delprat, "Low-frequency components and modulation processes in compressible cavity flows," *Journal of Sound and Vibration*, 2010, doi: 10.1016/j.jsv.2010.05.013.

[5] G. A. Brés and T. Colonius, "Three-dimensional instabilities in compressible flow over open cavities," *Journal of Fluid Mechanics*, 2008, doi: 10.1017/S0022112007009925.

[6] L. Larchevêque, P. Sagaut, T. H. Lê, and P. Comte, "Large-eddy simulation of a compressible flow in a three-dimensional open cavity at high Reynolds number," *Journal of Fluid Mechanics*, 2004, doi: 10.1017/S0022112004000709.

[7] J. Basley, L. R. Pastur, F. Lusseyran, J. Soria, and N. Delprat, "On the modulating effect of three-dimensional instabilities in open cavity flows," *Journal of Fluid Mechanics*, 2014, doi: 10.1017/jfm.2014.576.

[8] M. A. Kegerise, E. F. Spina, S. Garg, and L. N. Cattafesta, "Mode-switching and nonlinear effects in compressible flow over a cavity," *Physics of Fluids*, 2004, doi: 10.1063/1.1643736.

[9] D. Bacci, A. J. Saddington, and D. Bray, "Identification of the formation of resonant tones in compressible cavity flows," *Aerospace Science and Technology*, vol. 77, 2018, doi: 10.1016/j.ast.2018.03.013.

[10] M. B. Tracy and E. B. Plentovich, "Cavity unsteady-pressure measurements at subsonic and transonic speeds," *NASA Technical Paper*, 1997.

[11] C. Kannepalli, C. Chartrand, R. Birkbeck, N. Sinha, and N. Murray, "Computational Modeling of Geometrically Complex Weapons Bays," in *17th AIAA/CEAS Aeroacoustics Conference (32nd AIAA Aeroacoustics Conference)*, American Institute of Aeronautics and Astronautics, 2011. doi: doi:10.2514/6.2011-2774.

[12] L. Ukeiley, M. Sheehan, F. Coiffet, F. Alvi, S. Arunajatesan, and B. Jansen, "Control of pressure loads in geometrically complex cavities," 2008. doi: 10.2514/1.33324.

[13] M. F. Barone and S. Arunajatesan, "A Computational Study of Flow Within Cavities with Complex Geometric Features," in *53rd AIAA Aerospace Sciences Meeting*, American Institute of Aeronautics and Astronautics, 2015. doi: doi:10.2514/6.2015-0008.

[14] K. M. Casper, J. L. Wagner, S. J. Beresh, J. Henfling, R. Spillers, and B. O. Pruett, "Complex Geometry Effects on Open Cavity Dynamics," in *32nd AIAA Applied Aerodynamics Conference*, American Institute of Aeronautics and Astronautics, 2014. doi: doi:10.2514/6.2014-3025.

[15] K. M. Casper, J. L. Wagner, S. J. Beresh, R. Spillers, and J. Henfling, "Unsteady Pressure Sensitive Paint Measurements of Resonance Properties in Complex Cavities," in *46th AIAA Fluid Dynamics Conference*, American Institute of Aeronautics and Astronautics, 2016. doi: doi:10.2514/6.2016-3315.

[16] S. J. Lawson and G. N. Barakos, "Computational Fluid Dynamics Analyses of Flow over Weapons-Bay Geometries," *Journal of Aircraft*, vol. 47, no. 5, pp. 1605–1623, Sep. 2010, doi: 10.2514/1.C000218.

[17] D. Bacci, A. J. Saddington, and D. Bray, "Wavelet analysis of complex-geometry transonic cavity flows," 2016.

[18] L. L. Shaw, “Suppression of aerodynamically induced cavity pressure oscillations,” *Journal of the Acoustical Society of America*, 1979, doi: 10.1121/1.383242.

[19] E. F. Sheta, R. E. Harris, E. A. Luke, B. George, and L. S. Ukeiley, “Loads and Acoustics Prediction on Deployed Weapons Bay Doors,” in *33rd AIAA Applied Aerodynamics Conference*, American Institute of Aeronautics and Astronautics, 2015. doi: doi:10.2514/6.2015-3018.

[20] L. Daumas, F. Chalot, V. Levasseur, M. Mallet, and N. Reau, “LES and DES Aeroacoustic Simulations for Inflght opened Weapon Bay,” 2009.

[21] A. B. Blair and R. L. Stallings, “Cavity door effects on aerodynamic loads of stores separating from cavities,” *Journal of Aircraft*, vol. 26, no. 7, pp. 615–620, Jul. 1989, doi: 10.2514/3.45811.

[22] D. Bacci, A. J. Saddington, and D. Bray, “The effect of angle of attack on the aeroacoustic environment within the weapons bay of a generic UCAV,” *Aerospace Science and Technology*, vol. 93, p. 105315, 2019, doi: 10.1016/j.ast.2019.105315.

[23] G. J. M. Loupy, G. N. Barakos, and N. J. Taylor, “Cavity Flow over a Transonic Weapons Bay During Door Operation,” *Journal of Aircraft*, vol. 55, no. 1, pp. 339–354, Aug. 2017, doi: 10.2514/1.C034344.

[24] Y. Egorov, F. R. Menter, R. Lechner, and D. Cokljat, “The scale-adaptive simulation method for unsteady turbulent flow predictions. part 2: Application to complex flows,” *Flow, Turbulence and Combustion*, 2010, doi: 10.1007/s10494-010-9265-4.

[25] F. R. Menter, “Best Practice: Scale-Resolving Simulations in ANSYS CFD, Ver. 2.00,” 2015. doi: 10.1155/2013/859465.

[26] R. Chaplin and T. Birch, “The Aero-Acoustic Environment Within the Weapons Bay of A Generic UCAV,” in *30th AIAA Applied Aerodynamics Conference*, American Institute of Aeronautics and Astronautics, 2012. doi: doi:10.2514/6.2012-3338.

[27] M. J. de C. Henshaw, “M219 cavity case: Verification and validation data for computational unsteady aerodynamics,” in *Tech. Rep. RTO-TR-26, AC/323(AVT)TP/19*, 2002.

[28] S. J. Lawson and G. N. Barakos, “Evaluation of DES for weapons bays in UCAVs,” *Aerospace Science and Technology*, vol. 14, no. 6, pp. 397–414, Sep. 2010, doi: 10.1016/J.AST.2010.04.006.

[29] W. Clough, R. and J. Penzien, *Dynamics of Structures*. Mc-Graw-Hill, New York, USA, 1975.

[30] P. D. Welch, “The Use of Fast Fourier Transform for the Estimation of Power Spectra: A Method Based on Time Averaging Over Short, Modified Periodograms,” *IEEE Transactions on Audio and Electroacoustics*, 1967, doi: 10.1109/TAU.1967.1161901.